Microstructural Modification of 2-1/4 Cr-1 Mo Steel by Irradiation with 14 MeV Nickel Ions

R.L. Sindelar, J.J. Kai, D.L. Plumton, R.A. Dodd and G.L. Kulcinski

October 1985

UWFDM-667

Presented at the 1985 TMS-AIME Fall Meeting, 13-17 October 1985, Toronto, Ontario.

FUSION TECHNOLOGY INSTITUTE

UNIVERSITY OF WISCONSIN

MADISON WISCONSIN

"LEGAL NOTICE"

"This work was prepared by the University of Wisconsin as an account of work sponsored by the Electric Power Research Institute, Inc. ("EPRI"). Neither EPRI, members of EPRI, the University of Wisconsin, nor any person acting on behalf of either:

"a. Makes any warranty or representation, express or implied, with respect to the accuracy, completeness, or usefulness of the information contained in this report, or that the use of any information, apparatus, method, or process disclosed in this report may not infringe privately owned rights; or

"b. Assumes any liabilities with respect to the use of, or for damages resulting from the use of, any information, apparatus, method or process disclosed in this report."

Microstructural Modification of 2-1/4 Cr-1 Mo Steel by Irradiation with 14 MeV Nickel Ions

R.L. Sindelar, J.J. Kai, D.L. Plumton, R.A. Dodd
and G.L. Kulcinski

Fusion Technology Institute
University of Wisconsin
1500 Engineering Drive
Madison, WI 53706

http://fti.neep.wisc.edu

October 1985

UWFDM-667

Presented at the 1985 TMS-AIME Fall Meeting, 13-17 October 1985, Toronto, Ontario.

MICROSTRUCTURAL MODIFICATION OF 2 1/4 Cr-1 Mo STEEL BY IRRADIATION WITH 14 MeV NICKEL IONS

R.L. Sindelar, J.J. Kai, D.L. Plumton,
R.A. Dodd and G.L. Kulcinski

Fusion Technology Institute
Nuclear Engineering Department
University of Wisconsin, 1500 Johnson Drive
Madison, Wisconsin USA 53706

November 1985

UWFDM-667

Abstract

A ferritic steel (2 1/4 Cr-1 Mo) was heat-treated to produce three distinct microstructural regions: upper bainite, lower bainite and ferrite. The irradiation response of these different microstructures at 500°C to 14 MeV nickel ion irradiation was studied under identical conditions. Damage levels ranged from 80 dpa at the 1 μm depth to 350 dpa at the peak damage depth at 2.1 μm. Irradiated samples were studied in cross section using TEM/AEM thin foil techniques supplemented by precipitate extraction methods. The irradiation drastically changed the type of precipitate in the bainite regions from M_3C carbides to radiation-enhanced M_2C and M_7C_3 carbides and the radiation-induced χ-phase was also observed. The radiation-induced G-phase was the only precipitate type formed in the initial ferrite structure. No voids were observed up to 350 dpa in any of the three microstructures unless preinjected helium was present. An average swelling of 0.2% was measured after a dose of 100 dpa in the sample preimplanted to 100 appm helium.

Work supported by EPRI, Contract No. RP1597-2.

1. Introduction

Ferritic and martensitic steels are currently among the leading candidates for the cladding and ducts of fast breeder reactors and for the first wall and structural materials in conceptual fusion reactor designs [1]. In addition to their good mechanical properties during irradiation [2] and superior thermal stress resistance compared to the austenitic steels, ferritic steels seem to exhibit much better resistance to void swelling during neutron [3] and ion bombardment [4]. Unfortunately, this trend of lower swelling has not been established at dose levels much greater than 100 displacements per atom (dpa).

This study was initiated to study the microstructural stability, including precipitation response and void swelling characteristics, of a 2 1/4 Cr-1 Mo ferritic steel after a high temperature (500°C) and high dose (up to 350 dpa) ion irradiation. The use of the cross-section procedure and precipitate extraction methods unique to this study have clearly illustrated the dramatic effect of the ion bombardment on its triplex microstructure.

2. Experimental

2.1 Materials and Heat Treatment

The elemental composition (weight percent) of the 2 1/4 Cr-1 Mo steel used in this study is listed in Table 1. This reference heat of the alloy was provided by the Office of Fusion Energy and it was thermally treated at the Hanford Engineering Development Laboratory to produce a triplex microstructure.

The pre-irradiation heat treatment of a 3 cm thick steel plate consisted of a water quench after austenitizing for 1 hour at 1000°C, then tempering at 840°C for 2 hours and again water quenching. The martensite which formed on

quenching from 1000°C was transformed to a ($\alpha + \gamma$) structure upon tempering at 840°C, and the ferrite formed at this temperature was retained as such upon quenching. Presumably, both upper and lower bainite formed from the austenite phase during the final quench. Figure 1 displays extraction replica micrographs of the three preirradiation structures contained in the steel.

2.2 Irradiation Procedure and Analysis

Two samples of the steel were irradiated at 500°C with 14 MeV nickel ions in the University of Wisconsin tandem accelerator facility. Both were heat-treated as described above, but one was subsequently uniformly pre-implanted with 100 atomic parts per million (appm) helium to a depth of 1.3 μm using 200-700 keV helium ions in the University of Wisconsin hydrogen and helium accelerator facility. The damage profile created by 14 MeV nickel ions incident on a 2 1/4 Cr-1 Mo target is shown in Fig. 2. Both samples were irradiated to a fluence of 25 x 10^{16} ions/cm^2 at a nominal rate of 3 x 10^{11} ions/cm^2/s which corresponds to a displacement rate of ~ 1 x 10^{-3} dpa/s at a depth of 1 μm and ~ 4 x 10^{-3} dpa/s at a depth of 2.1 μm, the peak damage depth. The corresponding dose values at 1 μm and 2.1 μm were 80 and 350 dpa respectively.

Preparation of the samples for post-irradiation analysis involved the cross-section technique described in detail elsewhere [5]. This procedure allows the entire 3 μm damage region (see Fig. 2) to be viewed in a single transmission electron microscopy (TEM) specimen. In addition, precipitate extraction replicas [6] were prepared from the cross-sectioned samples in order to obtain accurate quantitative analyses [7] of the precipitates formed during the irradiation. The analytical electron microscopy was performed using a JEOL TEMSCAN 200CX electron microscope equipped with a Tracor-Northern TN 2000 energy dispersive x-ray analysis system.

3. Results

The irradiation caused profound changes in the precipitate type, morphology, and density in all three structures, while the thermal control region beyond the 3 μm damage range did not exhibit any evidence of tempering. In addition, a network dislocation structure of density ~ 3 x 10^{10} cm^{-2} was observed throughout the damage range. A slight increase in this density (~ 4 x 10^{10} cm^{-2}) occurred in the helium preinjection regions, but there was no distinguishable difference in the precipitate characteristics as a result of the helium preinjection.

A very striking result was the complete lack of void formation in all three microstructural regions of 2 1/4 Cr-1 Mo after irradiation in excess of 350 dpa in the absence of helium. The preinjection with 100 appm helium resulted in 0.2% average swelling after a dose of 100 dpa. This was accomplished by measuring void densities in several TEM specimens of known thickness.

3.1 Precipitation Response

Figure 3 shows a thin foil TEM micrograph which spans the entire damage range of a region of the 2 1/4 Cr-1 Mo steel which initially contained upper bainite. It can be seen that extensive restructuring of the upper bainite has occurred to a depth of ~ 3 μm from the surface of the irradiated sample. This corresponds well to the calculated damage range shown in Fig. 1. Figure 4 shows an enlarged view of this irradiated microstructure at the 1 μm depth (80 dpa), the 2.1 μm depth (350 dpa) and the thermal control region of the upper bainite (> 3 μm depth). The irradiation has nearly eliminated the lath structure of the upper bainite. In addition, the prior lath boundary Fe_3C has disappeared, and M_2C, M_7C_3, and χ phases were produced and identified from low-order zone diffraction patterns [8]. Their chemical analyses, obtained from

energy dispersive X-ray spectroscopy analysis of the extracted precipitates, are listed in Table 2. Both the M_7C_3 phase and the χ phase were of similar blocky or rod-like morphology and contained a similar iron and chromium content. After 350 dpa, very few of the small (~ 80 nm long) M_2C rods were observed and the M_7C_3 and χ precipitates were the dominant second phase particles.

Figure 5 shows the precipitate distribution at the 1 μm depth (80 dpa), the 2.1 μm depth (350 dpa) and the thermal control region of the lower bainite structure. The uniformly distributed Fe_3C rods in the original lower bainite structure no longer exist after a dose of 100 dpa. The blocky precipitates, which have replaced the cementite, were predominantly χ phase. At the 350 dpa damage level, this precipitate distribution was slightly more coarse than the distribution at 100 dpa.

Figure 6 displays the 1 μm, 2.1 μm depths, and the control region of the structure which was originally ferrite. Precipitates of similar morphology to the bainitic regions, but of a vastly different type, were produced in this region of the steel. Electron diffraction and EDS analysis of these precipitates on the extraction replica (shown in Fig. 7 and 8) were used to identify this phase as the G-phase, a nickel-rich silicide, commonly observed after neutron or ion-irradiation of several austenitic stainless steel alloys [9,10]. No other types of precipitates formed in the ferrite region.

There was little depth (dose) dependency in the precipitate size and number density in each of the three regions. Table 2 includes the average size and number density of the precipitates in each of the three regions. It is interesting to note that the densities do not vary appreciably with dose (depth), dropping by less than a factor of two even though the damage level is over 10 times higher at the peak damage depth (~ 2.1 μm) compared with the

near surface depths (< 1 μm). If is also noted that the precipitate density in the helium-doped region is roughly the same as in the undoped specimen at the same damage level.

3.2 Swelling Response

No voids were observed in any structure of the helium-free specimen throughout the entire range of ion damage. This result is particularly significant considering that the material was damaged to levels approximating 400 dpa at the damage peak. Voids and helium bubbles were detected in the specimen preimplanted with 100 appm helium.

Figure 9 shows the through-range microstructure of the sample uniformly preinjected with 100 appm helium up to the first 1.3 μm of material. Several features of interest were noted in this specimen. In the region from the front face up to 0.7 μm only very small (< 10 nm) cavities were observed. Most of these are believed to be helium bubbles. In the region from 0.7 to 1.3 μm clusters of voids formed. In the region between 1.3 μm and the end of range, no voids formed.

A summary of these depth-dependent void parameters is given in Table 3. Two values of swelling are listed in this table; those associated with the local swelling in the vicinity of the heterogeneously nucleated clusters and those associated with the swelling if it was homogenized in the 0.3 μm bandwidth between 70 and 100 dpa. The reason for this heterogeneous clustering of voids may be due to the fact that the incubation dose is only slightly exceeded. It would be interesting to irradiate this He doped specimen to much higher damage levels (i.e. 350 dpa at 1 μm) to see if a more uniform microstructure could be observed.

4. Discussion

The variety of phases observed following the ion irradiation indicates that complex phase reactions have occurred in this alloy. The precipitation response summarized in Table 2 may be compared to the tempering chart compiled by Nutting [11] for a 2 1/4 Cr-1 Mo steel, shown in Fig. 10. First, it is predicted that no tempering of the unirradiated control structures should occur at 500°C, in agreement with observations of the control region after the ~ 30 hours of irradiation time at 500°C. Second, the irradiation appears to have accelerated the carbide evolutionary sequence as the more mature carbides, M_2C and M_7C_3, have replaced the Fe_3C phase present in the original upper and lower bainite structures. This carbide distribution of M_2C and M_7C_3 would normally form during aging at temperatures in excess of 600°C for the period of irradiation. Third, the χ and G phases which formed in the original bainite and ferrite structures respectively during the irradiation do not appear on the tempering diagram. These radiation-induced phases have not been previously reported to form in irradiated 2 1/4 Cr-1 Mo steel.

The χ phase is an intermetallic compound which is commonly observed in aged austenitic stainless steel alloys [12]. It has been reported to replace the $M_{23}C_6$ carbide in a type 316 stainless steel weld metal with a duplex austenite-ferrite structure at high temperatures (> 700°C) as a result of an increase in the carbon solubility in the ferrite matrix [13]. There have been recent reports of χ phase formation during irradiation of HT-9, a high chromium ferritic alloy [14,15]. Kai [15] has observed this phase after ion-irradiation of HT-9 at 500°C.

The formation of G-phase in the original ferrite structure was not a totally unexpected result. This phase has formed during irradiation of type 316 stainless steels [9,10] as a result of strong defect-solute interactions

causing enrichment of nickel and silicon at microstructural defect sinks [16]. In this study, nickel has been implanted to nearly 5 atomic percent near the peak damage depths (Fig. 2). Simple calculations show that the nickel initially present in the alloy (0.16 wt.%) is sufficient to account for the nickel content of the G-phase at the 1 μm depth; at the 2.1 μm depth, however, the implanted nickel has undoubtedly been incorporated into this phase. Irradiations using an iron beam should be conducted to observe whether the G-phase will form in this alloy in the absence of the implanted nickel.

The low swelling results of this alloy during the ion-irradiation are consistent with the results from fast reactor irradiations. Gelles and Thomas [14] irradiated the same heat and initial structure of the 2 1/4 Cr-1 Mo steel in the Experimental Breeder Reactor II (EBR-II) up to fluence levels of 1.6 x 10^{23} n/cm^2 at a temperature of 425°C. Voids were observed at this fluence, but not at a lesser fluence of 5.1 x 10^{22} n/cm^2.

Figure 11 shows the average swelling rate determined in this study which suggests that the bulk-averaged rate of swelling is less than 0.01%/dpa. However, the local swelling rate is $\geq$ 0.01%/dpa. It is still noted, however, that the dose level (100 dpa) is probably not sufficient to establish the steady state [17] swelling rate.

5. Acknowledgements

The authors gratefully acknowledge the assistance of R.J. Schmidt, D.J. Pertzborn, L.E. Seitzman and D.H. Plantz during the high fluence irradiations. We also thank Dr. Nate Hoffman of ETEC for helpful comments during the course of this investigation.

References

[1] See Proceedings of: Topical Conference on Ferritic Alloys for use in Nuclear Energy Technologies, Eds. J.W. Davis and D.J. Michel, Snowbird, Utah, June 19-23, 1983.

[2] R.L. Klueh, J.M. Vitek and M.L. Grossbeck, J. Nucl. Mater. 103 & 104 (1981) 887.

[3] D.S. Gelles, J. Nucl. Mater. 122 & 123 (1984) 207-213.

[4] F.A. Smidt, Jr., P.R. Malmberg, J.A. Sprague and J.E. Westmoreland in Irradiation Effects on the Microstructure and Properties of Metals, ASTM STP 611, 1976, pp. 227-241.

[5] S.J. Zinkle and R.L. Sindelar, "Preparation of Ion-Irradiated Foils for Cross-Section Analysis," Proc. AIME Symposium on Irradiation Effects Associated with Ion Implantation, Toronto, 14-15 October, 1985. To be published in Nucl. Instr. & Methods.

[6] R.A. Dodd, details to be published in J. of Microscopy.

[7] N.J. Zaluzec in Introduction to Analytical Electron Microscopy, J.H. Hren, J.I. Goldstein and D.C. Joy (Eds.), Plenum Press, New York (1979) 121-167.

[8] K.W. Andrews, D.J. Dyson and S.R. Keown, in Interpretation of Electron Diffraction Patterns, Adam Hilger, Ltd., 2nd Ed., 1971.

[9] E.H. Lee, P.J. Maziasz and A.F. Rowcliffe, in Phase Stability During Irradiation, J.R. Holland, L.K. Mansur and D.I. Potter, Eds., p. 191, (1980).

[10] W.J.S. Yang, H.R. Brager and F.A. Garner in Ref. 9, p. 257.

[11] J. Nutting in Ref. 1, pp. 3-16.

[12] P. Marshall, Austenitic Stainless Steels: Microstructure and Mechanical Properties, Elsevier Applied Science Publishers, Ltd., (1984).

[13] J.K. Lai and J.R. Haigh, Welding Research Supplement, supplement to the Welding Journal, January 1979, 1s.

[14] D.S. Gelles and L.E. Thomas in Ref. 1, pp. 559-563.

[15] J.J. Kai, unpublished research.

[16] P.J. Maziasz, J. Nuc. Mater. 122 & 123 (1984) 472.

[17] F.A. Garner in Ref. 16, pp. 459-471.

Table 1. Composition of Fusion Heat of 2 1/4 Cr-1 Mo, Lukens Ht-C4337-14S, PIN-Code-A387-D, in Weight Percent

C	Cr	Mo	Mn	Ni	Si	P	S	Cu	Al	Fe
0.12	2.17	0.93	0.42	0.16	0.21	0.011	0.011	0.16	0.003	Bal.

Table 2. Precipitate Parameters of Ion-Irradiated 2 1/4 Cr-1 Mo Steel - 500°C

Original Structure	Irradiated Phases & Composition Determined by Energy Dispersive X-ray Analysis	Unirradiated Control	Dose (dpa)	Precipitate Size (nm)	Precipitate Number Density (10^{14} cm^{-3})
Upper Bainite	χ: 60 Fe-37 Cr-3 Mo	Fe_3C: 85 Fe-15 Cr	100	56 15 (M_2C)	4.1
	M_7C_3: 40 Fe-55 Cr-5 Mo		400	57	3.2
	M_2C: 10 Fe-55 Cr-35 Mo		Control	85	~ 5
Lower Bainite	χ. 60 Fe-37 Cr-3 Mo	Fe_3C: 85 Fe-15 Cr	100	25	10
	M_7C_3: 40 Fe-55 Cr-5 Mo		400	55	5.2
			Control	70	20
Ferrite	G: 25 Fe-20 Cr-15 Mo		100	39	3.8
	35 Ni-5 Si		400	50	2.7
			Control	---	---

Table 3. Cavity Characteristics of 2 1/4 Cr-1 Mo Bombarded with 14 MeV Ni Ions at 500°C After Preinjection with 100 appm He

Void density (0.3 μm, 50 dpa)	6×10^{14} cm^{-3}
(0.7-1.3 μm, 100 dpa)	2×10^{14} (Locally)
Average cavity diameter (0.3 μm, 50 dpa)	9 nm
(0.7-1.3 μm, 100 dpa)	38 nm
Average swelling (0.3 μm, 50 dpa)	0.03%
(0.7-1.3 μm, 100 dpa)	0.5% (Locally)
(0.7-1.3 μm, 100 dpa)	0.2% (Homogeneous)
Average bubble density (0.3 μm, 50 dpa)	8×10^{15} cm^{-3}
Average bubble diameter (0.3 μm, 50 dpa)	2 nm

Figure Captions

Fig. 1. Extraction replica micrographs of upper bainite, lower bainite and ferrite present in the 2 1/4 Cr-1 Mo steel aged at 840°C (2 hours) after a 1005°C solution quench.

Fig. 2. Damage (dpa) versus distance from the irradiated surface calculated using the Brice code. The damage efficiency (K) used is 0.8. E_d = 40 eV.

Fig. 3. Transmission electron micrographs spanning the entire damage region of 14 MeV Ni-ion irradiated 2 1/4 Cr-1 Mo which initially contained upper bainite. Note the drastic restructuring of the upper bainite throughout the entire 3 μm range of damage.

Fig. 4. TEM micrographs at the unirradiated thermal control region, 1 μm depth (80 dpa) and 2.1 μm depth (350 dpa) of the upper bainite structure. M_2C needles, M_7C_3 and χ-phase formed in this structure during the irradiation.

Fig. 5. TEM micrographs at the unirradiated thermal control region, 1 μm depth (80 dpa) and 2.1 μm depth (350 dpa) of the lower bainite structure. Both χ-phase and M_7C_3 precipitates formed in this structure during the irradiation.

Fig. 6. TEM micrographs at the unirradiated thermal control region, 1 μm depth (80 dpa) and 2.1 μm depth (350 dpa) of the ferrite structure. The nickel and silicon enriched G-phase was the predominant second phase particle in the irradiated ferrite.

Fig. 7. Extraction replica micrograph which shows the precipitation response in the 3 μm damage range has been severely altered from the precipitate distribution of the unirradiated structures. Note that the vast restructuring has occurred in each (upper bainite, lower bainite, ferrite) region.

Fig. 8. Extraction replica micrographs and the EDS spectra of the radiation-induced χ-phase and G-phase. The χ-phase formed in the bainitic regions while the G-phase formed in ferrite during the nickel-ion irradiation of 2 1/4 Cr-1 Mo.

Fig. 9. TEM micrographs spanning the entire damage region of the 2 1/4 Cr-1 Mo sample which had been implanted to 100 appm He up to the 1.3 μm depth. A clustering of voids occurred at various locations at the ~ 1 μm depth (100 dpa). A more uniform cavity/bubble distribution was observed at near surface depths (0.3-0.7 μm).

Fig. 10. Tempering diagram for 2 1/4 Cr-1 Mo steel reported by Nutting [11].

Fig. 11. Swelling characteristics of the ion-irradiated 2 1/4 Cr-1 Mo. The local swelling was determined in the vicinity of a cluster of voids; the homogeneous swelling was the total swelling which occurred at a particular depth (dose).

FIGURE 1

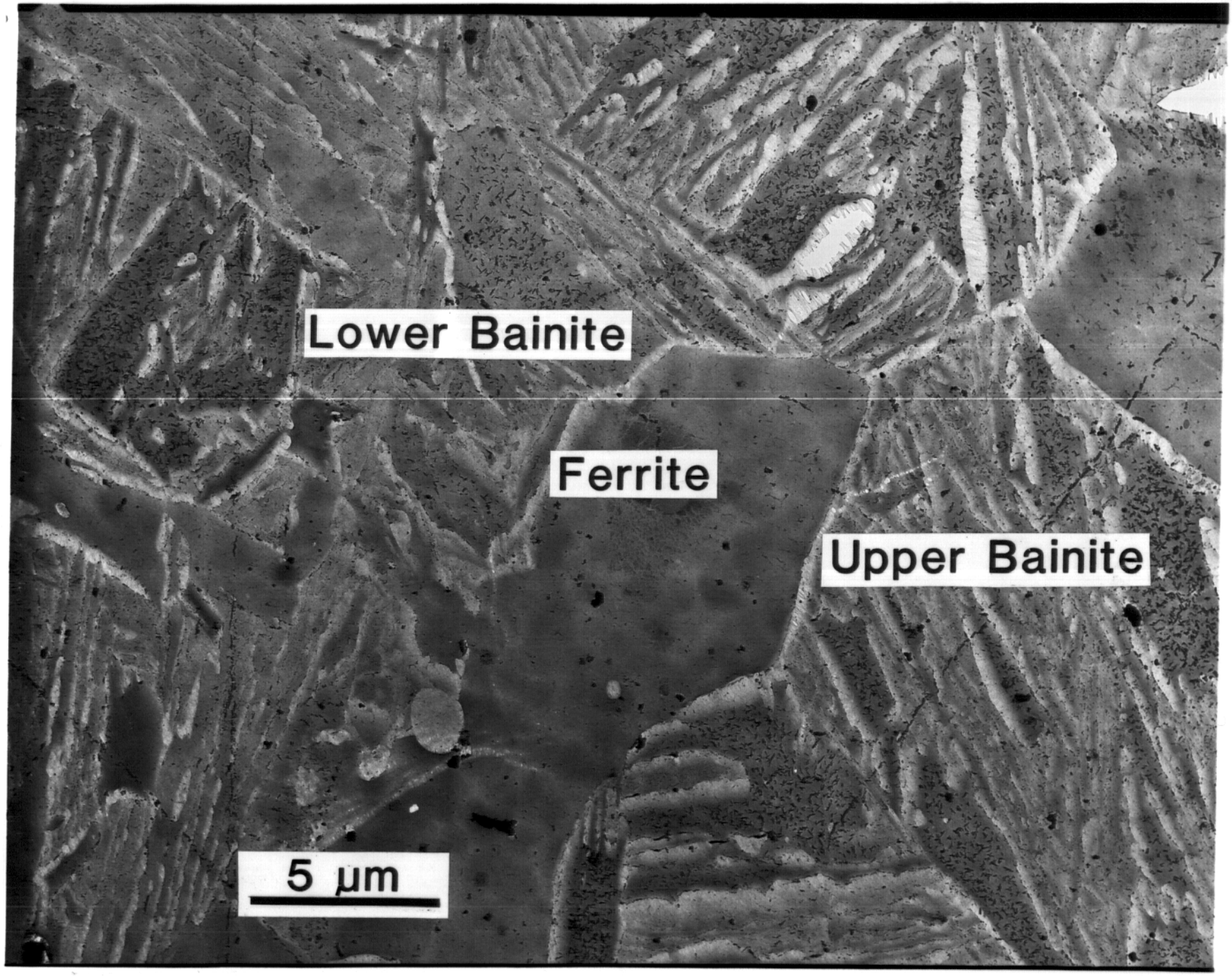

FIGURE 2

Displacement Damage and Implanted Ion Concentration versus the Incident Ion Range

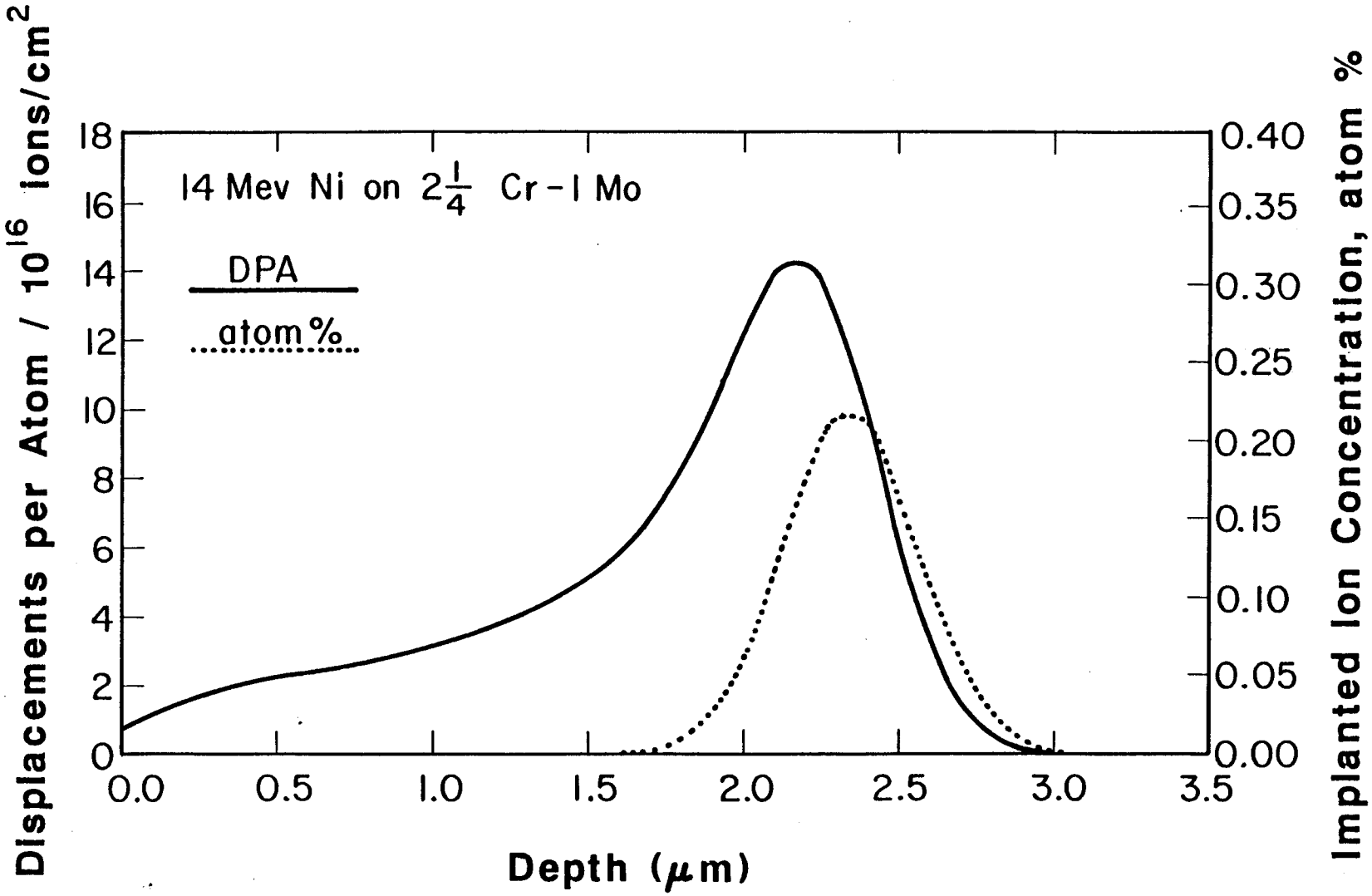

14 MeV Ni-ION-IRRADIATED 2 1/4Cr 1Mo

THROUGH-RANGE MICROSTRUCTURE

FIGURE 4

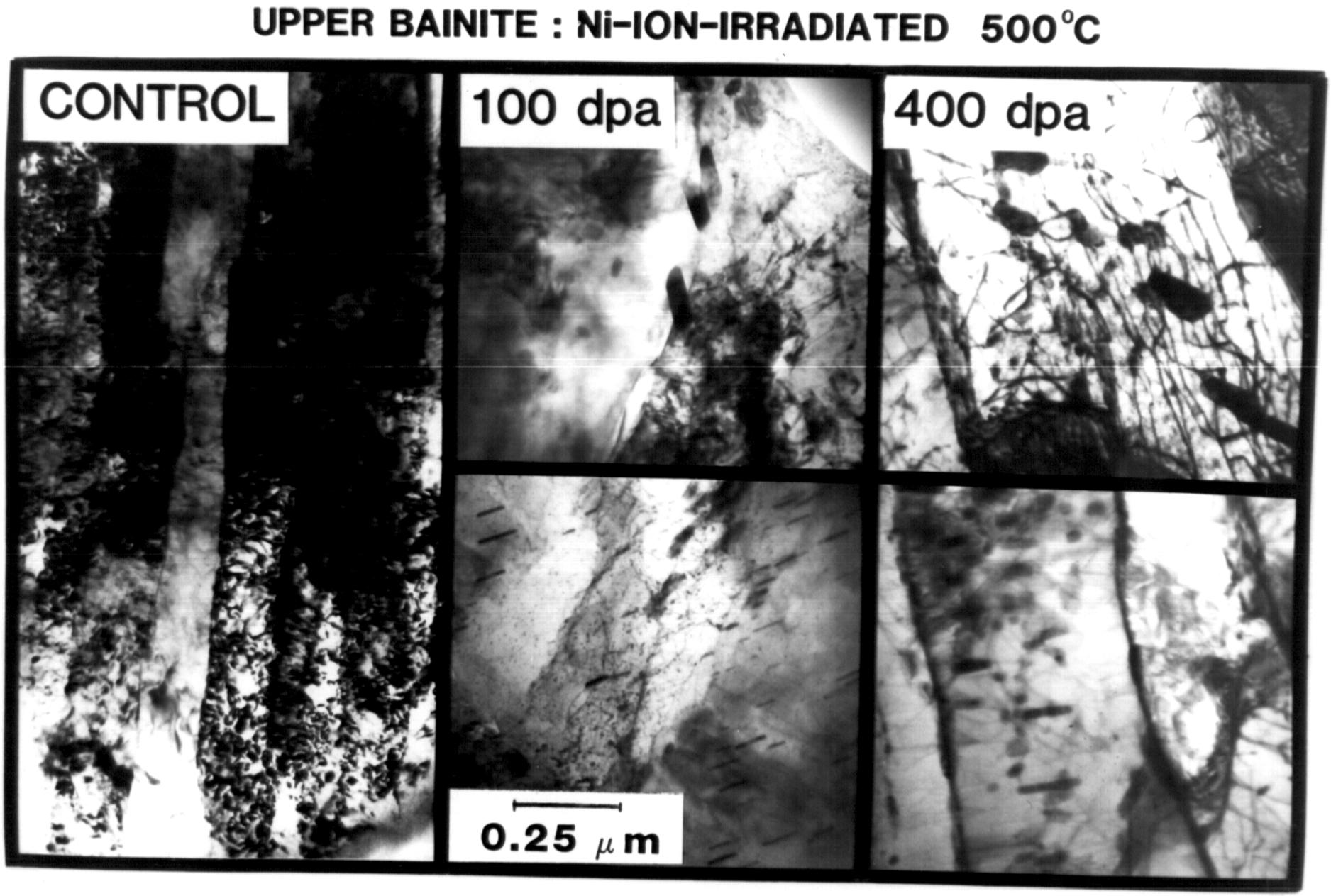
UPPER BAINITE : Ni-ION-IRRADIATED 500°C
CONTROL
100 dpa
400 dpa
0.25 μm

FIGURE 5

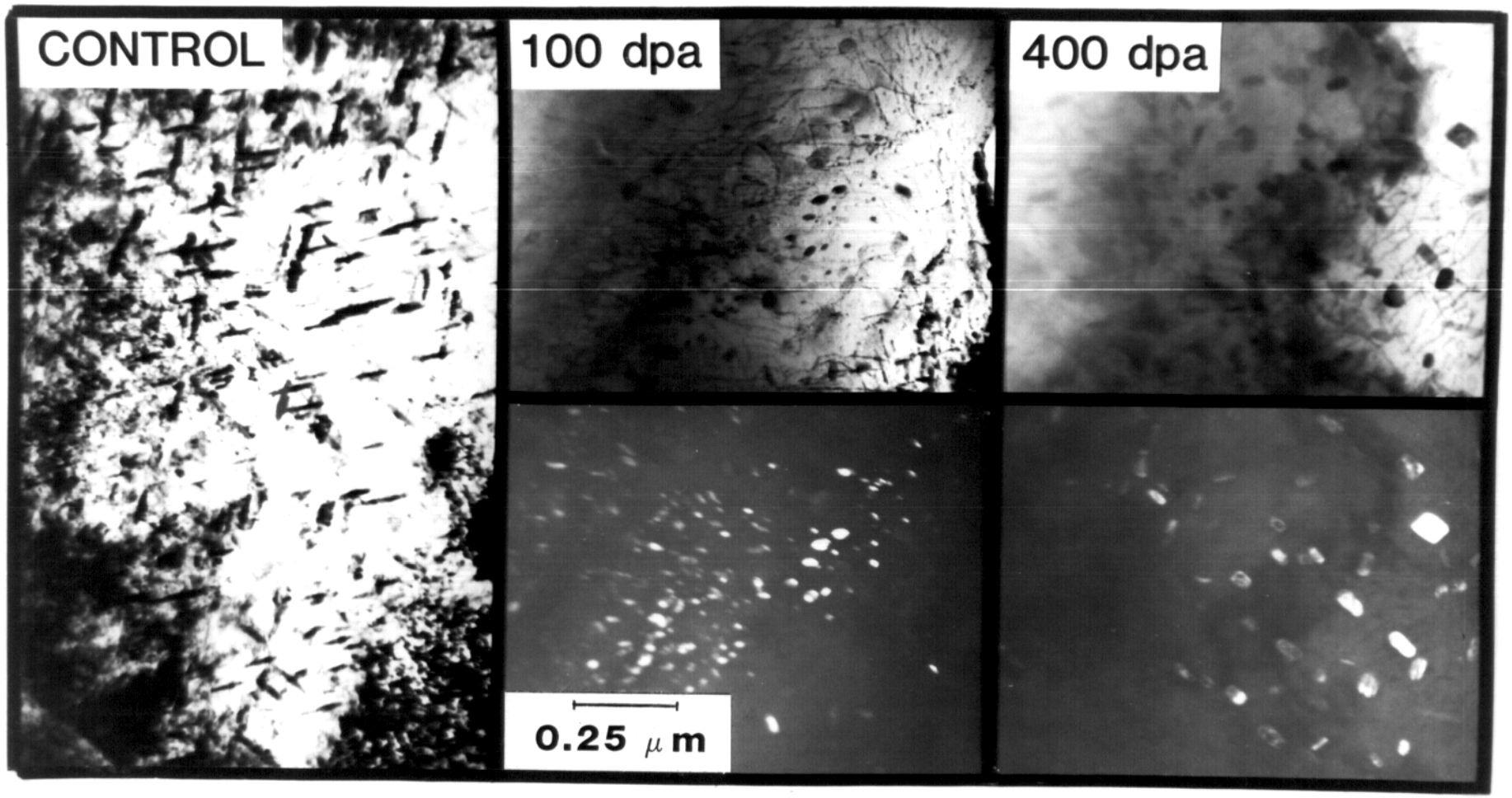
LOWER BAINITE : Ni-ION-IRRADIATED 500°C
CONTROL
100 dpa
400 dpa
0.25 μm

FIGURE 6

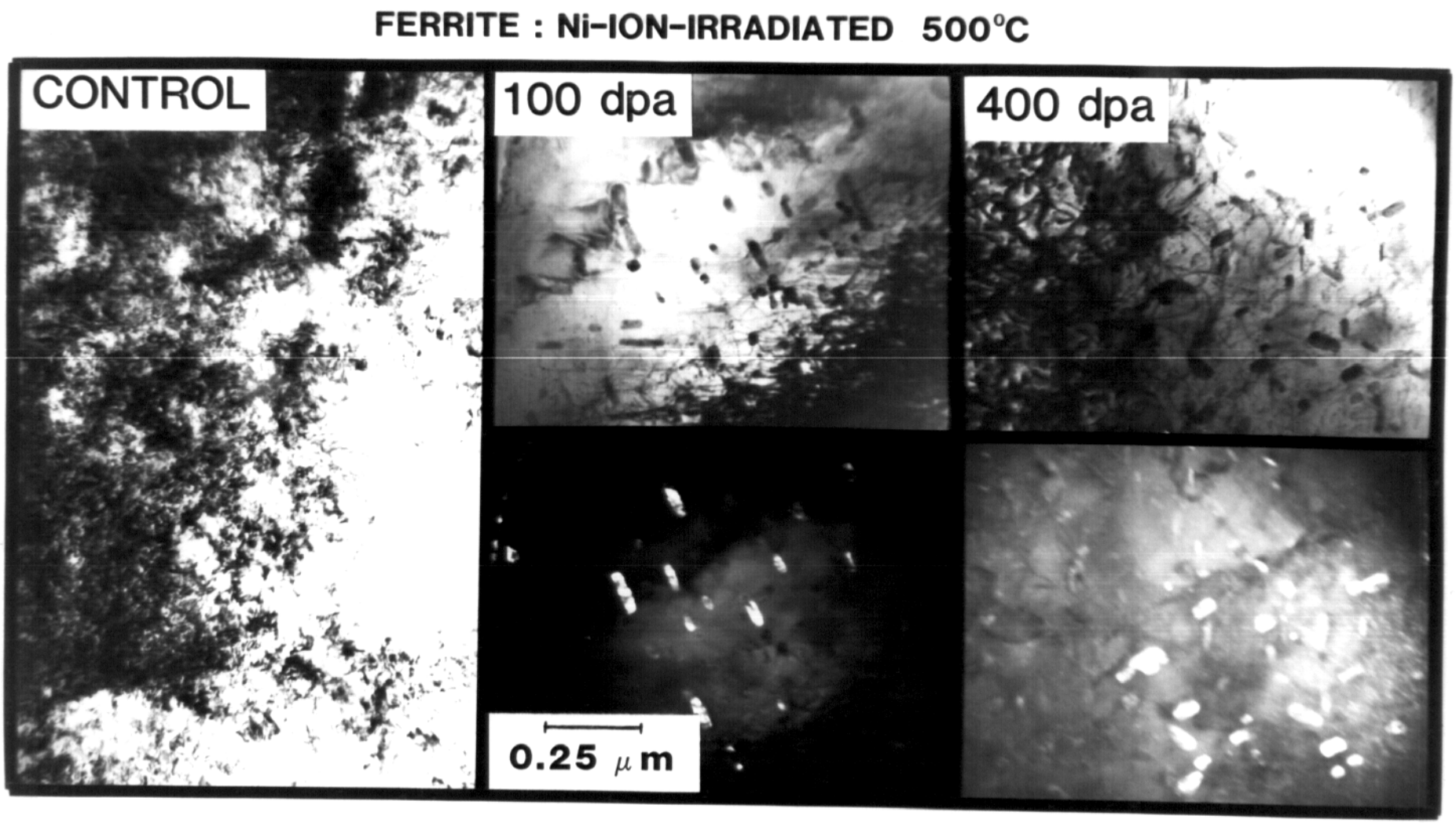
FERRITE : Ni-ION-IRRADIATED 500°C
CONTROL
100 dpa
400 dpa
0.25 μm

FIGURE 7

Extraction Replica Ion-Irradiated 2 1/4 Cr - 1 Mo

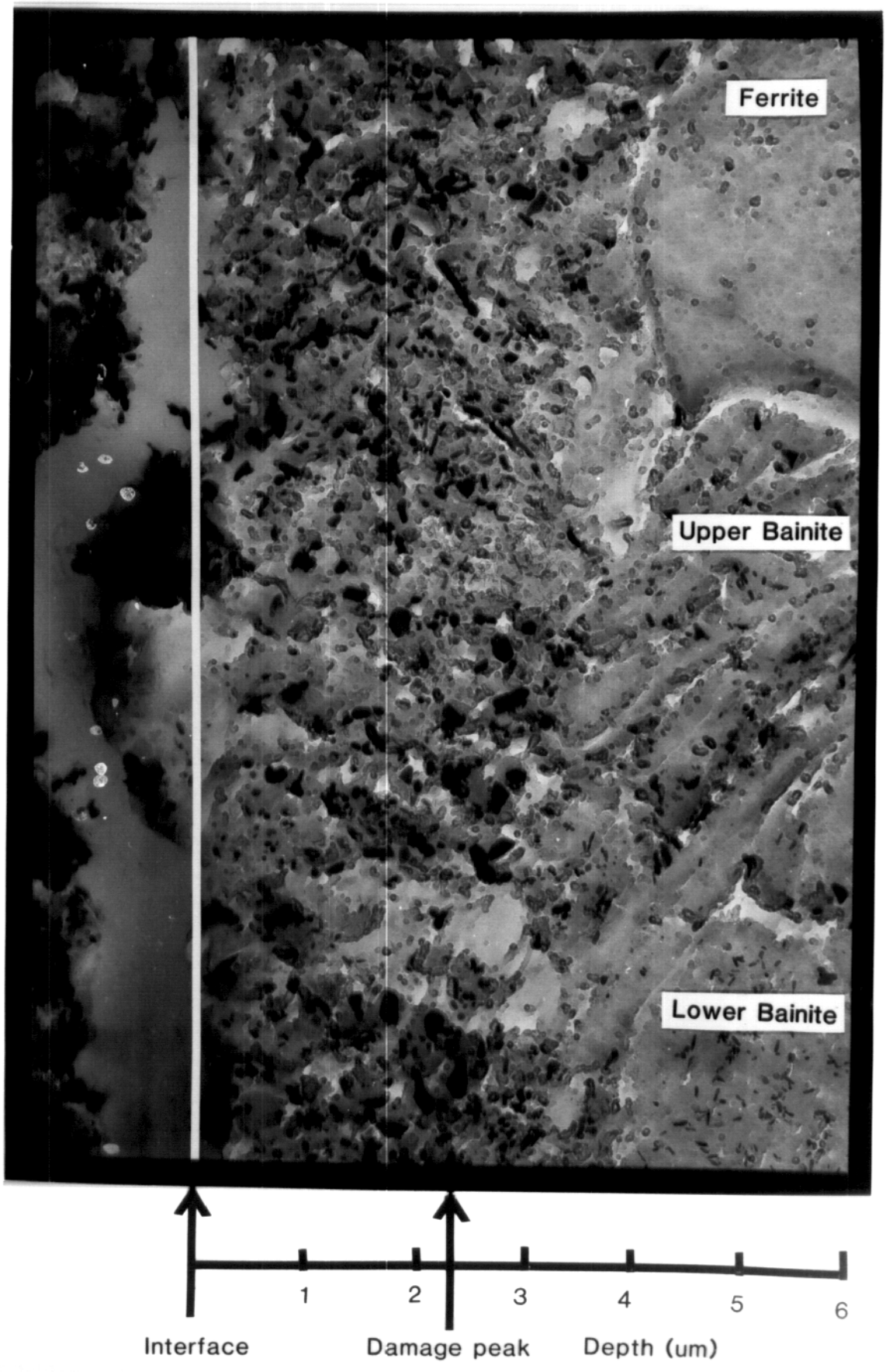

FIGURE 8

2 1/4 Cr – 1 Mo Ion-Irradiated, 500 °C
Radiation-Induced ppt. , Extraction Replica

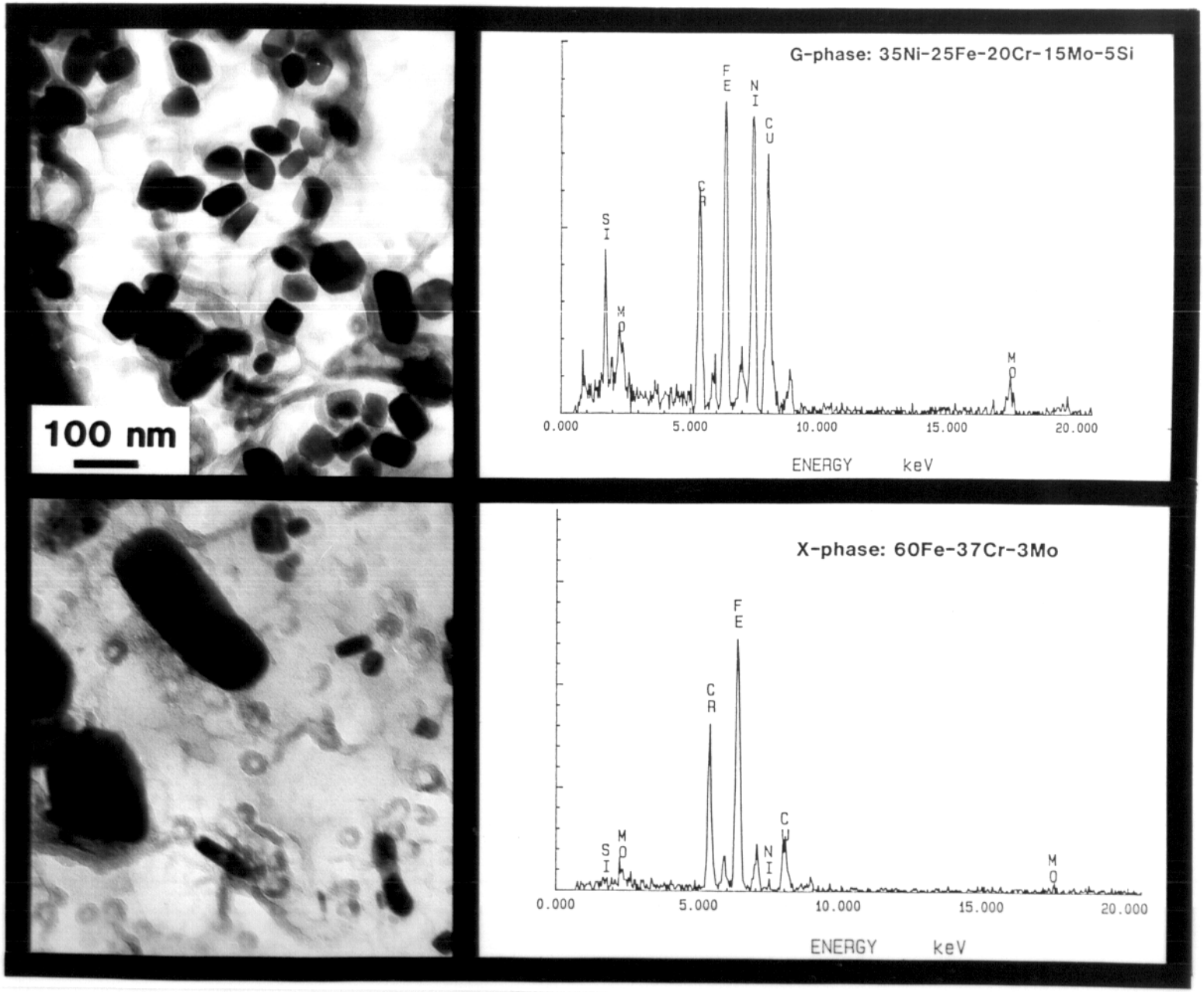

FIGURE 9

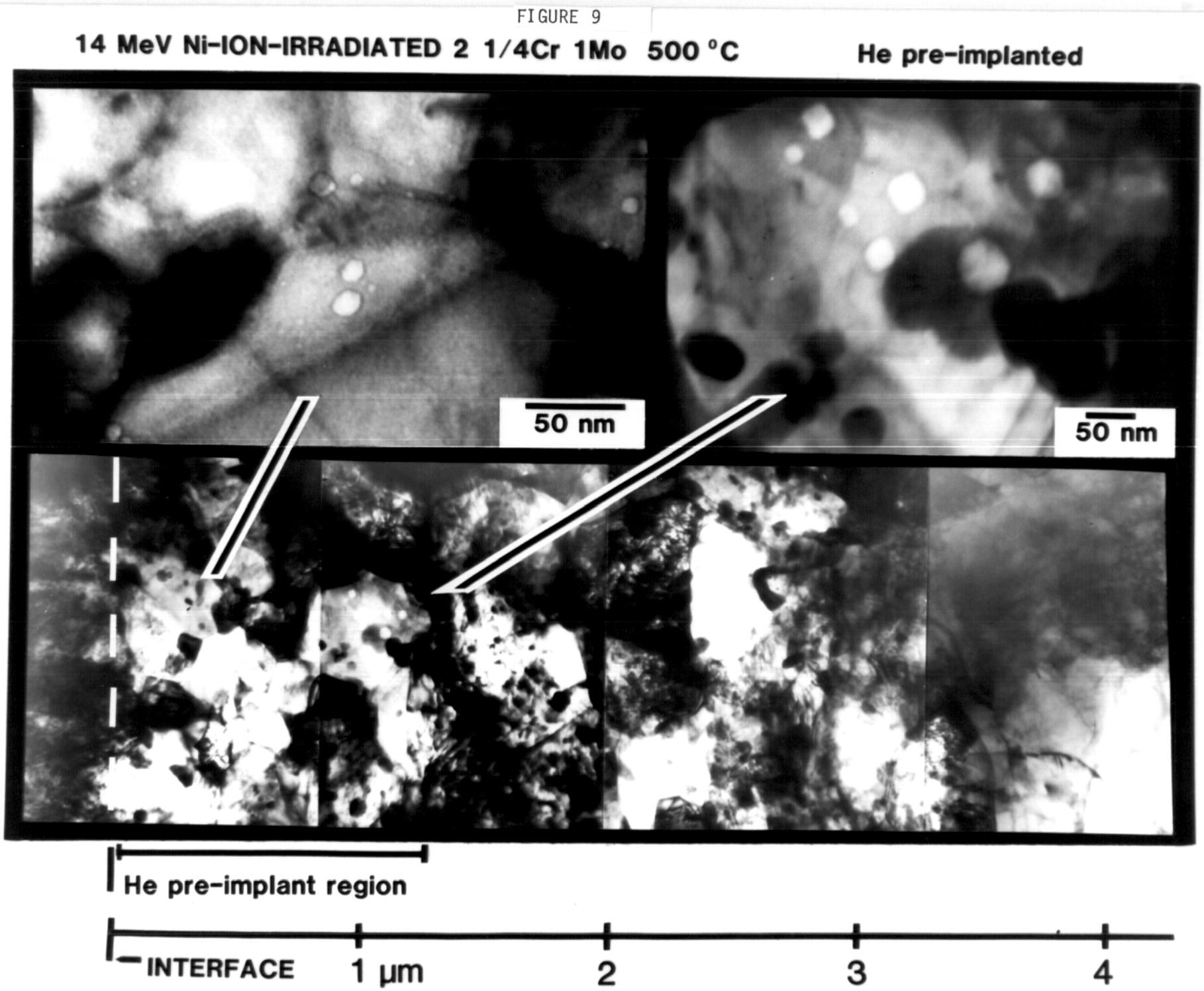
14 MeV Ni-ION-IRRADIATED 2 1/4Cr 1Mo 500 °C
He pre-implanted
50 nm
50 nm
He pre-implant region
INTERFACE
1 μm
2
3
4

FIGURE 10

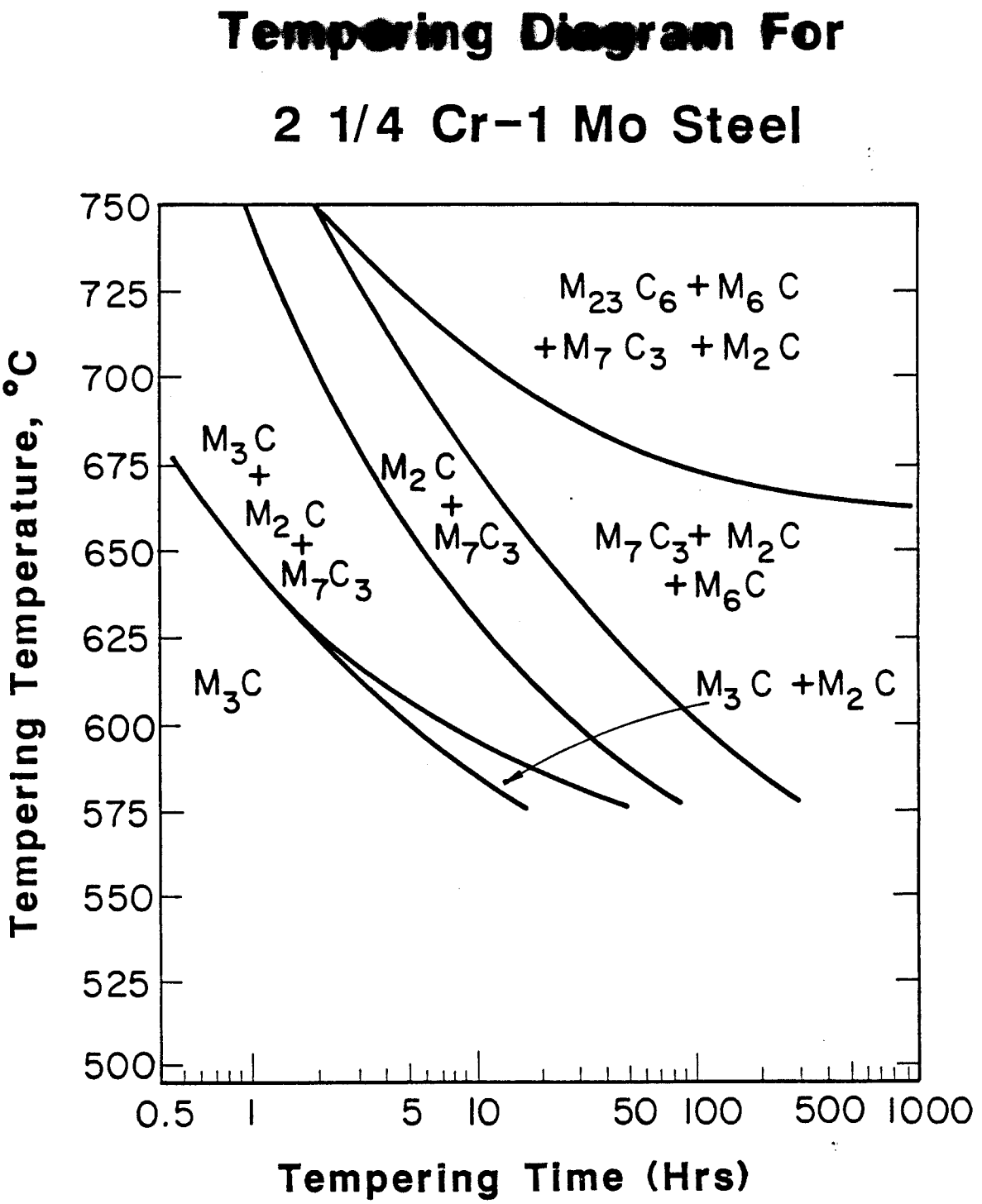
Tempering Diagram For
2 1/4 Cr-1 Mo Steel
Tempering Temperature, °C
750
725
700
675
650
625
600
575
550
525
500
0.5
1
5
10
50
100
500
1000
Tempering Time (Hrs)
M23 C6 + M6 C
+ M7 C3 + M2 C
M3C
+
M2 C
+
M7C3
M2 C
+
M7C3
M7 C3+ M2C
+M6C
M3C
M3 C +M2 C

FIGURE 11

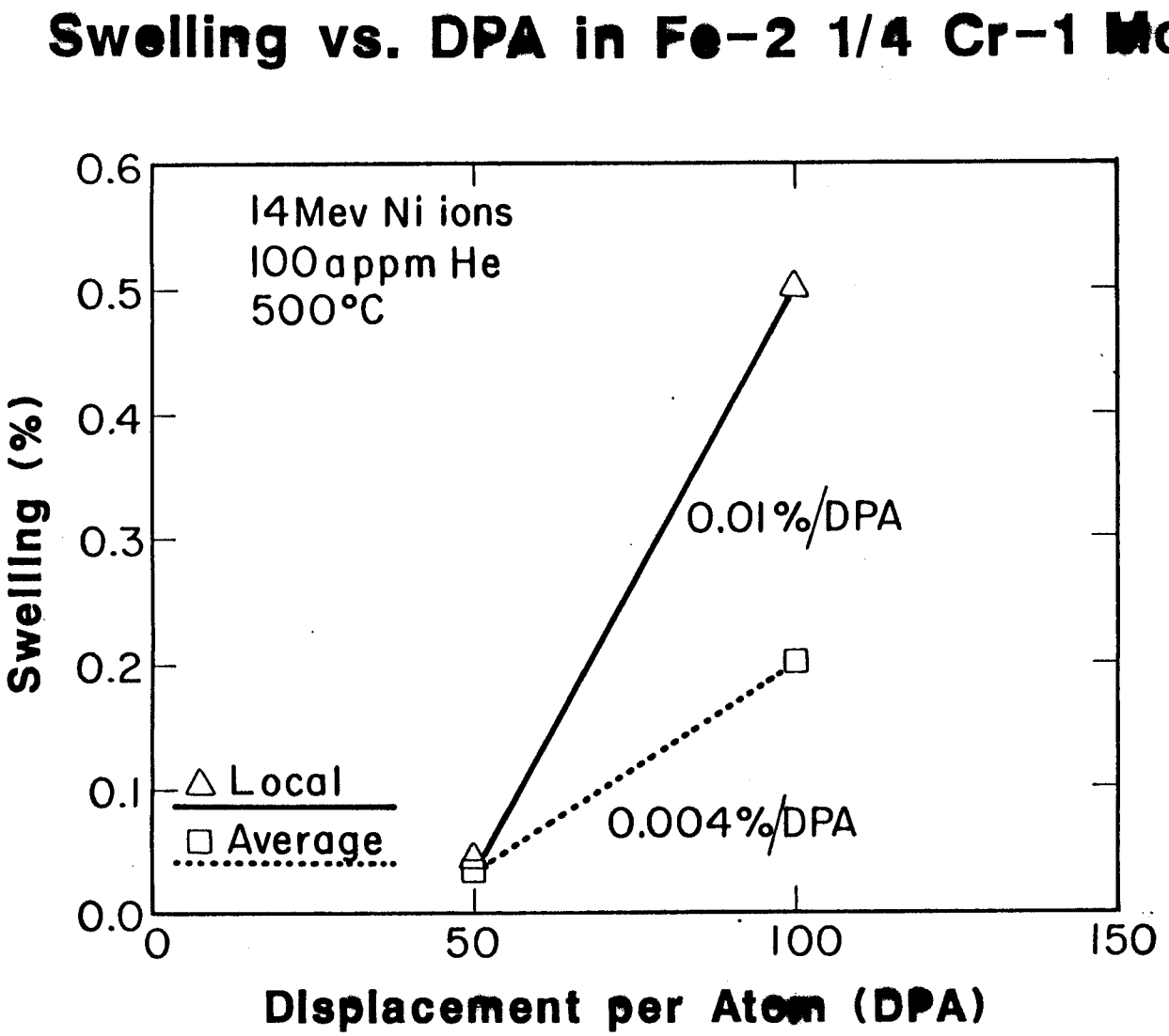
Swelling vs. DPA in Fe-2 1/4 Cr-1 Mo
14Mev Ni ions
100appm He
500°C
0.01%/DPA
0.004%/DPA
△ Local
□ Average
Swelling (%)
0.0
0.1
0.2
0.3
0.4
0.5
0.6
0
50
100
150
Displacement per Atom (DPA)